JOURNAL OF GEOPHYSICAL RESEARCH, VOL. 96, NO. A7, PAGES 11,421–11,439, JULY 1, 1991

ISEE 1 Observations of Electrostatic Ion Cyclotron Waves in Association With Ion Beams on Auroral Field Lines From ~2.5 to 4.5 R_E

C. A. CATTELL,[1] F. S. MOZER,[1,2] I. ROTH, [1], R. R. ANDERSON,[3]
R. C. ELPHIC,[4,5] W. LENNARTSSON,[6] AND E. UNGSTRUP[7]

Quasi-monochromatic waves at ~1.2 f_{cH}, where f_{cH} is the hydrogen cyclotron frequency, were observed as the ISEE 1 satellite traversed auroral field lines at radial distances of ~2.5–4.5 R_E near midnight on June 19, 1981. The waves were polarized perpendicular to the magnetic field ($k_\parallel/k_\perp \leq 0.2$). In addition, there were waves at slightly above both the helium and the oxygen cyclotron frequencies. The waves occurred within a region of reduced density (~0.1–0.2/cm^3) with the electron temperature greater than the ion temperature, upflowing hydrogen and oxygen beams, and weak field-aligned currents bounded by electrostatic shocks. The wave characteristics and associations were similar to those observed at lower altitudes by the S3-3 satellite. Comparisons were made between the observed H^+ and O^+ beams, field-aligned currents, densities and temperatures, and linear theories of electrostatic ion cyclotron waves and H^+-O^+ two-stream instabilities. The features of the observed waves are most consistent with the current-driven mode. In addition, numerical studies of the linear dispersion relation, using parameters based on the observations, showed that both the parallel and oblique two-stream modes and the ion-beam driven modes were stable while oblique current driven modes were unstable. The O^+ and H^+ distributions provide evidence for interactions with local electrostatic ion cyclotron waves and for the H^+-O^+ two-stream instability at altitudes below the satellite.

1. INTRODUCTION

Since the suggestion of *Kindel and Kennel* [1971] that field-aligned currents should drive electrostatic ion cyclotron waves (EIC) in the auroral zone, the occurrence of this wave mode, its source of free energy, its effects on both ions and electrons, and its importance in auroral phenomenology have been studied extensively using rocket, satellite, and laboratory experiments, theoretical analysis, and computer simulations. Observational data on EIC waves were obtained by the S3-3 satellite, and to date, only electrostatic hydrogen cyclotron waves (EHC) have been identified in that data set. Characteristics of the waves, including frequency, wave number, and waveform [*Kintner et al.*, 1978, 1979; *Temerin et al.*, 1979; *Kintner*, 1980], and the association of the waves with ion beams [*Kintner et al.*, 1979], field-aligned currents [*Cattell*, 1981], and other auroral phenomena [*Cattell*, 1984; *Temerin and Mozer*, 1984] have all been described. Similar associations of ion beams and hydrogen cyclotron waves have been observed at higher altitudes by DE 1 [*Kintner et al.*, 1983] and Viking [*André et al.*, 1987]. In contrast, both hydrogen and oxygen cyclotron waves have been reported in rocket data [*Bering et al.*, 1975; *Kelley et al.*, 1975; *Bering*, 1984; *Kintner et al.*, 1989, and references therein]. Two possible sources of free energy for EIC waves have been identified: ion beams and field-aligned currents. Analytical and simulation studies of both beam- and current-driven modes have been made [*Kindel and Kennel*, 1971; *Ashour-Abdalla and Thorne*, 1978; *Kaufmann and Kintner*, 1982, 1984; *Miura et al.*, 1983; *Bergmann*, 1984; *André*, 1985], including the effects of the waves on both electrons and ions [*Hudson et al.*, 1978; *Ungstrup et al.*, 1979; *Lysak et al.*, 1980; *Dusenbery and Lyons*, 1981; *Ashour-Abdalla et al.*, 1981; *Ashour-Abdalla and Okuda*, 1984]. In addition, there are nonlinear methods for exciting EIC waves such as three-wave decay [*Bergmann*, 1986] and radiation by ion holes [*Tetreault*, 1991]. Laboratory plasma studies have also addressed these phenomena [*Böhmer et al.*, 1976; *Hauck et al.*, 1978; and references therein]. The free energy source and the complex relationship between EIC waves and auroral zone dynamics, however, are still not understood.

More recently, attention has focused on the interaction of oxygen and hydrogen beams drifting relative to one another (rather than a single ion beam drifting relative to the electrons or background ions) [*Bergmann and Lotko*, 1986; *Kaufmann et al.*, 1986; *Bergmann et al.*, 1988; *Dusenbery et al.*, 1988; *Roth et al.*, 1989]. Waves in the same frequency range and with similar wave vectors to EIC waves can be produced by the ion two-stream interaction in certain parameter regimes.

In this paper we focus on one event where quasi-monochromatic waves at approximately the hydrogen cyclotron frequency were observed as ISEE 1 traveled down along auroral field lines from ~4.5 to ~2.5 R_E. The satellite track and a schematic representation of selected data quantities are shown in Figure 1. Waves at both lower (around the hydrogen gyrofrequency) and higher (above the hydrogen gyrofrequency) frequencies were observed at higher altitudes, and possible electrostatic helium cyclotron and oxygen cyclotron waves occurred at lower altitudes. Upflowing hydrogen and oxygen beams and field-aligned currents occurred simultaneously. Using data from the small burst memory of the spherical double-probe experiment (which sampled the electric field at frequencies below 128 Hz), the ion mass spectrometer data, the dc electric and magnetic fields, the high-frequency (10^2–4×10^5 Hz) electric field from the swept frequency receiver, the electric spectrum analyzer (5.6 Hz to 311 kHz), and the electron spectrometer, the following topics will be examined: (1) the large-scale morphol-

[1]Space Sciences Laboratory, University of California at Berkeley.
[2]Also at Physics Department, University of California at Berkeley.
[3]Department of Physics and Astronomy, University of Iowa, Iowa City.
[4]Now at Los Alamos National Laboratory, Los Alamos, New Mexico.
[5]Institute of Geophysics and Planetary Physics, University of California, Los Angeles.
[6]Lockheed Palo Alto Research Laboratory, Palo Alto, California.
[7]Danish Space Research Institute, Lyngby.

Paper number 91JA00378.
0148-0227/91/91JA-00378$05.00

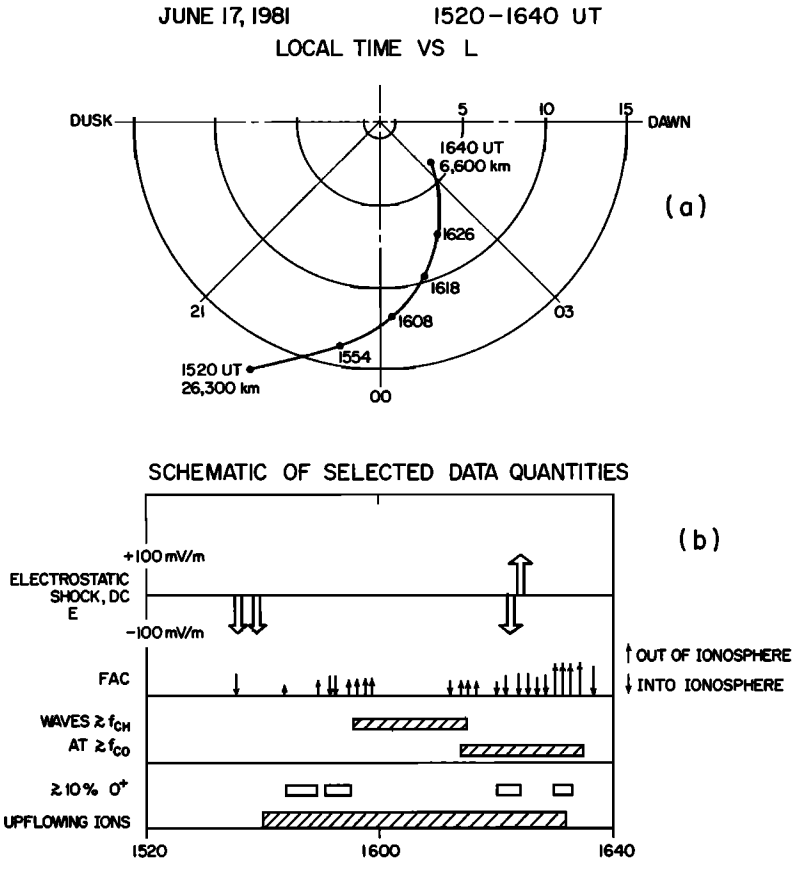

Fig. 1. *(a)* The satellite track in L-LT coordinates for the event. *(b)* A schematic model of some important data quantities. The overall structure of the event is very similar to the electrostatic shock events observed at lower altitudes by the S3-3 satellite.

ogy of the event; (2) the characteristics of the EIC waves; (3) wave/particle interactions; (4) free energy sources; and (5) the relationship to higher-frequency waves.

The instrumentation and data sets are described in section 2, the large-scale morphology is presented in section 3 and the low frequency waves in section 4, free energy sources are examined in section 5, the effects of the waves on ions are discussed in section 6, and discussion and conclusions are in section 7.

2. Instrumentation and Data Sets

The dc and low-frequency ac electric field data were obtained from the University of California, Berkeley, double-probe experiment on ISEE 1 [*Mozer et al.*, 1978]. This study concentrates on the electric field from 2 to 128 Hz measured by the burst mode of the instrument which made 128 samples of the electric field along the spinning booms in 0.5 s every 128 s. In addition, the dc 3-s spin period averages of the GSE x and y components of the field, the spacecraft potential (which is indicative of the plasma density), and the outputs of three broad filters will be described. Verification of instrument operation in low-density plasmas and error sources in the electric field measurement are discussed in *Mozer et al.* [1983] and *Pedersen et al.* [1984].

The ion data were obtained by the Lockheed energetic ion mass spectrometer on ISEE 1 [*Shelley et al.*, 1978]. During this period the instrument was operated in a special mode, designed to study the auroral acceleration region, in which pitch angle scans of both H^+ and O^+ were obtained at eight energies (0.21–17.4 keV) every 64 s (see *Sharp et al.* [1983] for details).

The electron data are from the ISEE 1 electron spectrometer [*Ogilvie et al.*, 1978] which was operating in a mode which measured electrons from 105 to 7050 eV. Nine-second averages of the density and temperature and distribution functions will be shown. During this period, detector 1, the poleward detector, was not operating. This has minimal effect on the density and temperature moments; however, velocity moments and therefore the current carried by the electrons could not be calculated accurately.

The magnetic field data are from the University of California, Los Angeles, flux gate magnetometers on ISEE 1 [*Russell*, 1978]. High time resolution data (4 points per second) will be shown. To determine field-aligned currents, the data were rotated into a dipole coordinate system, and the background field was removed. ISEE 2 data, which were available only during the first part of the event, were used to determine current sheet orientation and thickness.

High-frequency (>100 Hz) ac electric fields were obtained from the swept frequency receiver of the University of Iowa plasma wave experiment on ISEE 1 [*Gurnett et al.*, 1978]. A spectrum from 10^2 to 10^6 Hz was obtained every 32 s. In addition, the data from the electric spectrum analyzer with filters from 5.6 Hz to 311 kHz were examined. Note that it is difficult to see peaks below ~10 Hz in the spectrum analyzer due to solar array noise interference.

3. Event Overview

The large-scale morphology of the time period of interest (1520–1630 on June 19, 1981), which occurred as ISEE moved

in nearly along auroral field lines from an altitude of ~26,300 km to ~6600 km (~5.1–2 R_E geocentric), is presented schematically in Figure 1 (described above), and selected data are shown in Figure 2. During this period, ISEE moved from a dipole L of ~15 and local time of ~2245 to a dipole L of ~4 and local time of ~0300. From ~1535 to ~1630 the duskward (y GSE) component of the 3-s-averaged electric field (Figure 2*a*) was generally variable and ≤40 mV/m with the maximum field of ~100 mV/m occurring in a narrow spike at ~1623. If, however, the electric fields observed at ~1535 were mapped, assuming equipotential field lines, to the same altitude as those at ~1623, the magnitudes would be comparable. Examination of the raw electric field data shows that these large fields had a time scale of several spin periods, so that the spin period averaged data provide an accurate determination of the magnitude of the field in the spin plane. The x component (i.e., close to parallel to B) was always much smaller than the y component. Note that comparison with S3-3 data [*Mozer et al.*, 1980] suggests that

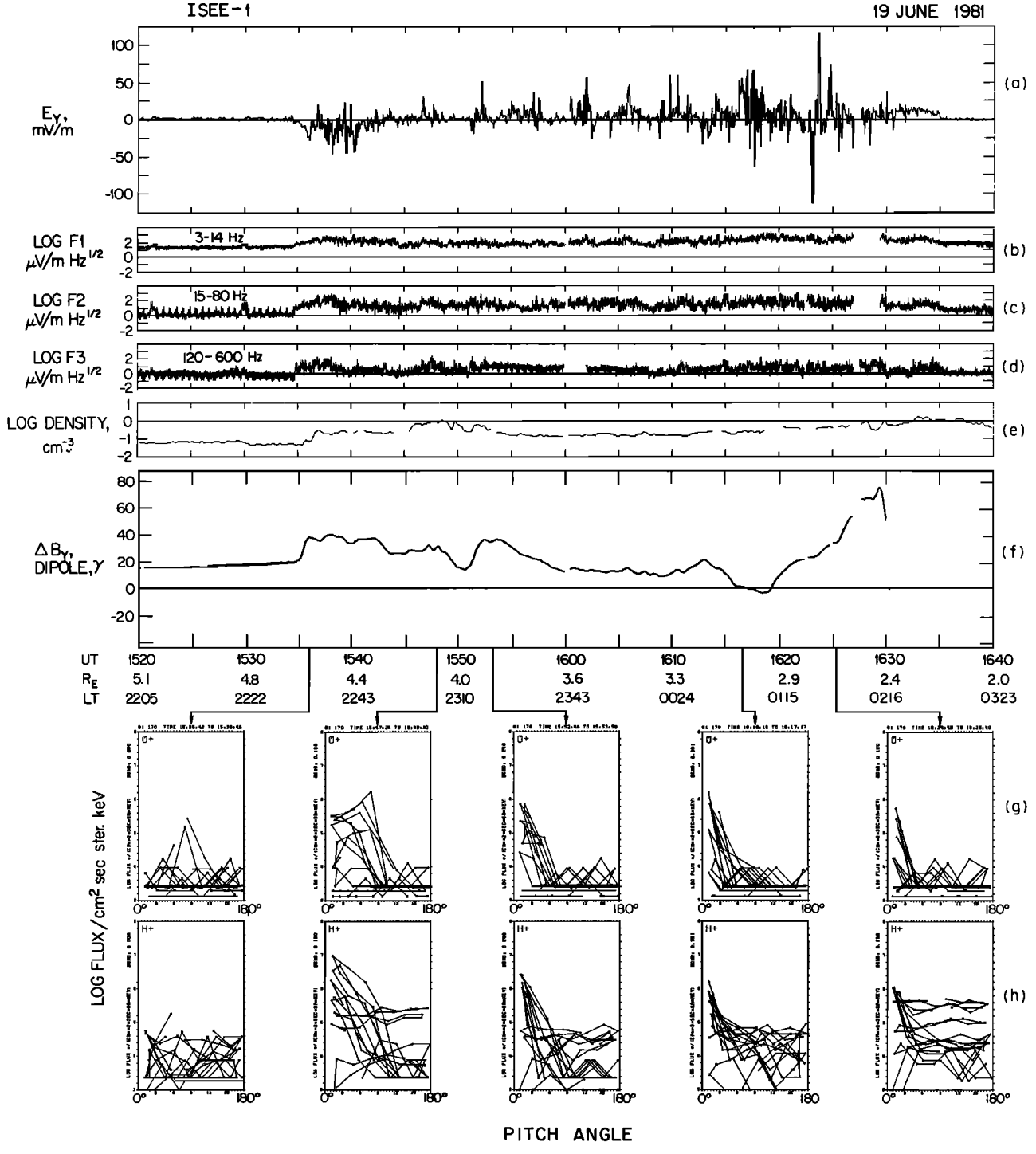

Fig. 2. An overview of the event on June 19, 1981: *(a)* the dawn-dusk component of the electric field, *(b)* the negative of the spacecraft potential which is indicative of the thermal plasma density, *(c)-(e)* the outputs of three broad filters, *(f)* the azimuthal perturbation in the magnetic field which indicates field-aligned currents, and *(g)* and *(h)* selected pitch angle distributions of O^+ and H^+, respectively.

the largest component of the electric field would be the GSE z component, which is not measured by the ISEE satellite. V_{2S}, the negative of the spacecraft potential (Figure 2*b*), indicates changes in the plasma density, since $V_{2S} \propto \log nT_e^{1/2}$ [*Mozer et al.*, 1983]. Density measurements will be discussed in more detail in section 5. There were two broad density depletions, from ~1535 to ~1545 and from ~1553 to ~1623, with another density increase at ~1630.

Figures 2*g* and 2*h* show selected pitch angle distributions of O^+ and H^+, respectively. Upflowing ions are peaked at 0° since the satellite was in the southern hemisphere. There were no fluxes above background until 1535:42, when the oxygen fluxes (215 and 400 eV) peaked near 90°. By 1538:54, both oxygen and hydrogen were upflowing (peaked at 10°, which was as close as the detector came to B). At ~1542 the O^+ became conical. The highest fluxes were observed from ~1546 to ~1553, when the O^+ was peaked at angles varying from ~45° to ~70° and the hydrogen peaked along the field. Ion beams with variable fluxes and maximum energies were observed in both oxygen and hydrogen throughout the time ~1552–~1633, with a second region of intense fluxes occurring from ~1615 to ~1625. From ~1618 to 1622 and from ~1625 to 1630 the distributions were more complex than simple upflowing beams.

The perturbation in the y component of the 4-s-averaged magnetic field in dipole coordinates (in which $\hat{z}$ is along the model field, $\hat{y}$ is azimuthal eastward, and $\hat{x}$ is in the magnetic meridian plane pointing southward) is shown in Figure 2*f*. Figure 3 shows both the x and the y components of the high-resolution magnetic field in field-aligned coordinates. Field-aligned current sheets extensive in longitude cause perturbations primarily in the y component. For the observed geometry and assumed satellite velocity with respect to the medium, increases (decreases) in B_y correspond to currents flowing toward (away from) the Earth. At ~1536 there was a current toward the Earth (~0.02 A/m), followed by several weaker currents, then an outward sheet of comparable size at ~1543, again followed by weaker currents and, finally, another more intense outward sheet at ~1548. At ~1552 the current was toward the Earth with a magnitude ~0.02 A/m; from ~1554 to ~1619 there was a weak (~0.03 A/m) current generally away from the Earth. The final three currents were the most intense and consisted of an inward current from ~1620 to ~1630 (~0.06 A/m), an outward current from ~1630 to ~1634 (0.09 A/m), and another inward current from ~1634–~1636. There may be some inaccuracies in the current determination after ~1610 because the satellite was moving rapidly in local time (i.e., parallel to the assumed current sheet) and the perturbation in the $\hat{x}$ component was becoming large. The fact that the perturbations in the x component were sometimes comparable to the y component perturbations indicates that the observed field-aligned currents are not well modeled by infinite sheet currents aligned along an L shell. ISEE 2 magnetic field data, available until 1539 UT, were used to determine current sheet thickness and current density. The main current at ~1536 had a thickness of ~490–590 km and a maximum current density of 60 nA/m^2 and was traveling outward (i.e., normal to the L shell) at a velocity of 4–6 km/s. Since the spacecraft are below the magnetic equator, this is a southward motion of the current sheet.

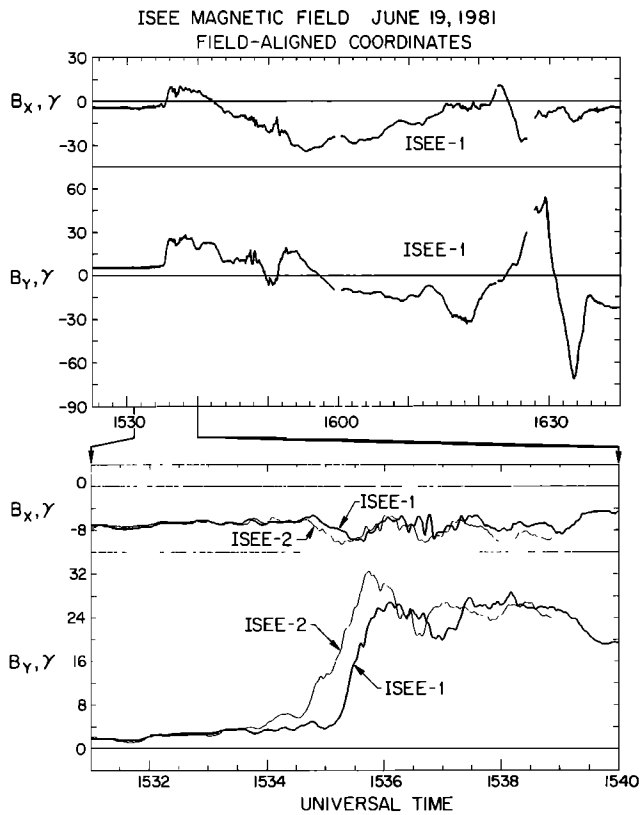

Fig. 3. The magnetic field in field-aligned components (in which the z axis is along the average field direction, and y is azimuthal). The x and y components of the magnetic field measured by ISEE 1 for the entire event are plotted in the top two panels. The bottom two panels show an expanded view of both the ISEE 1 and ISEE 2 magnetic field for the time period when ISEE 2 data were available.

Throughout the region of upflowing ions, density depletion, and large dc electric field, there were enhanced levels of low-frequency noise, as indicated in Figures 2*c*, 2*d*, and 2*e*, which plot the output from three broad filters. This morphology [large spiky electric fields (electrostatic shocks) bounding a region of depleted density, upflowing ion beams, and enhanced plasma waves] is the same as was observed on the S3-3 satellite at lower altitudes (5000–8000 km) [*Mozer et al.*, 1980; *Temerin et al.*, 1981; *Mizera et al.*, 1981; *Temerin and Mozer*, 1984]. Figure 5 of *Mozer et al.* [1979], Figure 7 of *Mozer et al.* [1980], and Figures 2 and 4 of *Mizera et al.* [1981] all present examples of these associations.

4. Wave Observations

The low-frequency electric field data which motivated this study are shown in Figures 4*a*, 4*b* and 4*c*. Each panel contains two consecutive 0.5-s electric field waveforms obtained in the burst mode.

The burst mode data for the initial 30 min of the period in Figure 2 are shown in Figure 4*a*. Waves above background were not observed until the onset of the field-aligned current, density decrease and large dc electric fields at ~1535. Dominant frequencies varied from $<f_{cH}$ to $\sim 8 f_{cH}$ or ~4–74 Hz (which for these samples also corresponded to peaks at $<f_{pi}$, the ion plasma frequency); the spectra were often very flat, and the range of amplitudes was large. One of the two largest amplitude samples occurred during this period, at ~1552, when the dominant frequency was approximately 3 times the hydrogen cyclotron frequency. From ~1600 to 1625 (Figure 4*b*), quasi-monochromatic waves at approximately f_{cH}, the hydrogen cyclotron frequency, with amplitudes of a few millivolts per meter are apparent in most of the samples in the upper four panels. In addition, waves at ~f_{cH} occurred in association with

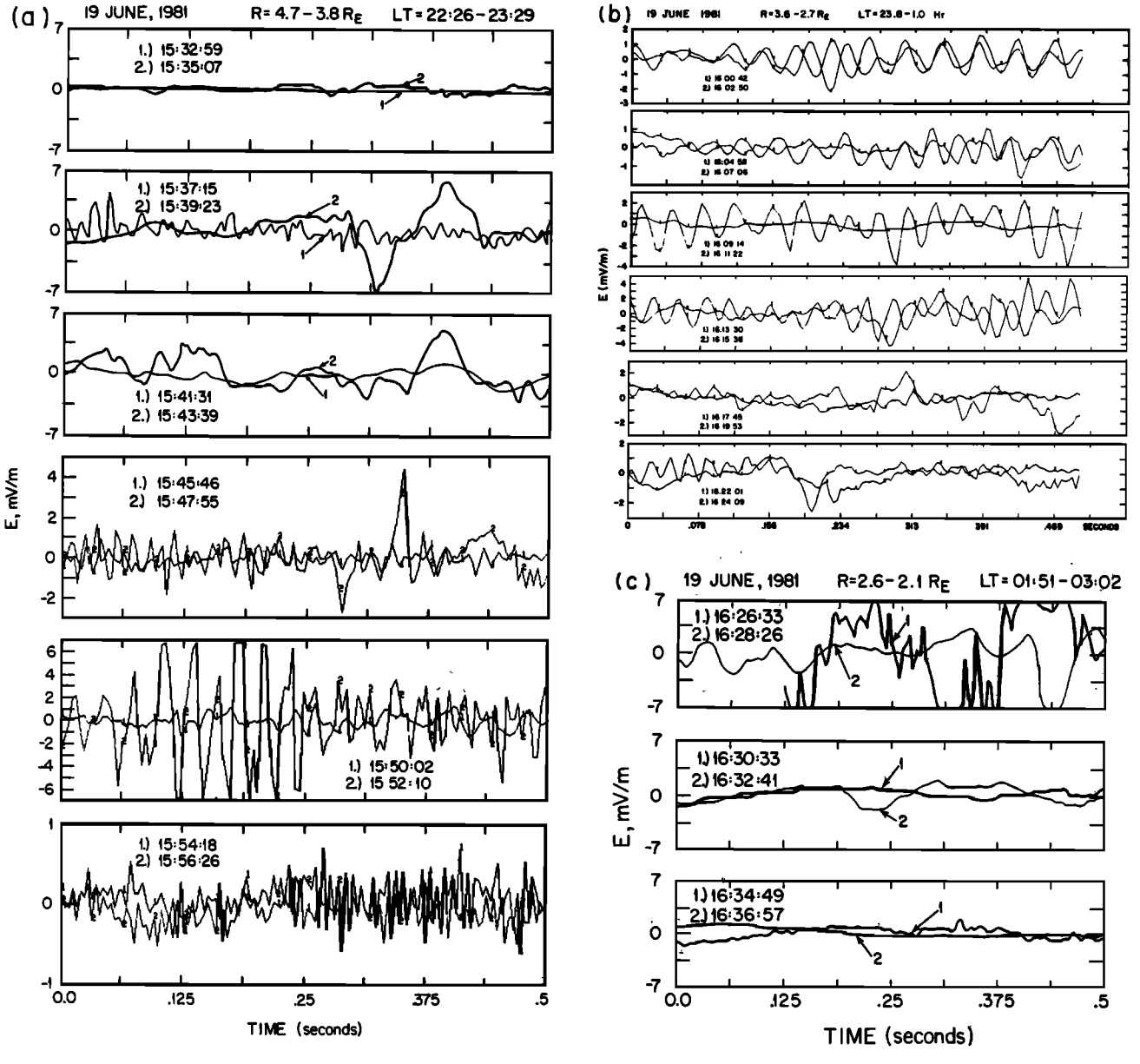

Fig. 4. The 0.5-s snapshots of the electric field along the spinning booms, taken in the burst mode of the instrument, for the period of the event.

waves at lower frequencies during the other samples in this figure. The waves shown in Figure 4*c* are basically similar to those observed during the preceding samples of Figure 4*b*. The waves in sample 1 (1626:33) were intense enough to saturate the measured quantity (±7 mV/m). Since there were missing data points during this burst, a spectrum was not computed, but by examination the dominant frequency was ~5 Hz or ~1.5 f_{cO} with some power occurring near f_{cH} also.

To determine the properties (f, k) of the waves, we have examined various characteristics of the waveforms, the power spectra, and the simultaneous filter data. For all cases when the peak power was $>10^{-2}$ $(mV/m)^2$ Hz^{-1} (for each sample in Figure 4 for which a Fourier spectrum could be calculated), the frequency at which the peak power was observed has been plotted as a circled dot versus the local hydrogen cyclotron frequency in Figure 5 (the corresponding universal time is also noted). Secondary peaks (power within a factor of 0.5 of the primary peak) have been plotted as crosses. The data from the University of Iowa spectrum analyzer generally agreed well with the peaks observed above ~10 Hz.

Before ~1600 the waves occurred over a broad frequency range, as discussed above. It can be seen that after ~1600 the frequencies at the peak power fall into three groups: one associated with the H^+ cyclotron frequency, one with the He^+ cyclotron frequency f_{cHe}, and one with the O^+ cyclotron frequency f_{cO}. This suggests that the observed waves may be electrostatic ion cyclotron waves which for brevity will be referred to as EHC, EOC, and EHeC below. Other wave modes, such as ion two-stream instabilities, can also have frequencies in this range. Note that it is difficult to be certain that the waves at $\gtrsim f_{cHe}$ are electrostatic He^+ cyclotron waves for several reasons: (1) the ion mass spectrometer was not in a mode to measure He^+, (2) f_{cHe} is also $(f_{cO}f_{cH})^{1/2}$, which is the two-ion hybrid frequency when the O^+ and H^+ densities are comparable, and (3) there are waves other than EHeC waves that have $f_{cHe} < f < f_{cH}$, such as the Alfvén ion cyclotron waves [*Lysak and Temerin*, 1983; *Temerin*

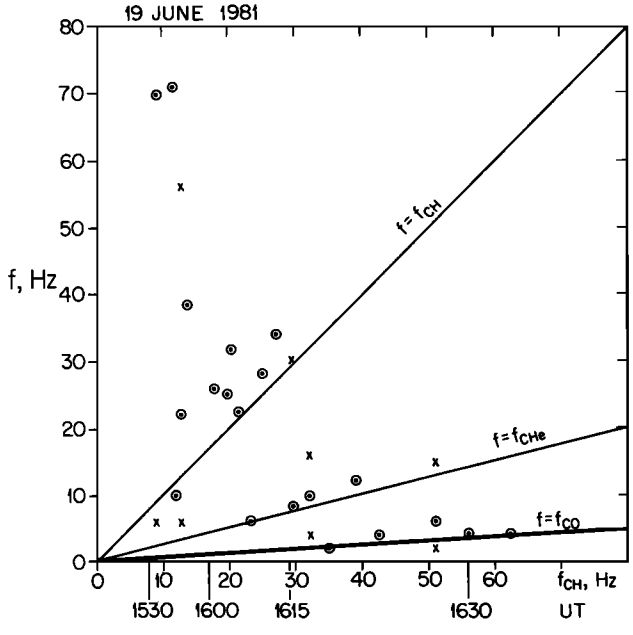

Fig. 5. The frequency at which the peak power (circled dot) occurred for each burst in figure for which a spectrum could be computed. Secondary peaks (with power within a factor of 0.5 of the primary peak) are indicated by a cross.

and Lysak, 1984], and ion two-stream instabilities [*Bergmann et al.*, 1988]. Indirect evidence for the existence of a population of He^+ can be obtained by comparing the density inferred after energy analysis and that after both energy and mass analysis (see Figure 6). At the times where the two are different (for example, at ~1620–1625 and 1543–1546 and other shorter intervals), He^+ may have been present. Ion densities were calculated under the assumption that the fluxes were gyrotropic in the instrument frame and varied linearly with energy between the energy channels sampled.

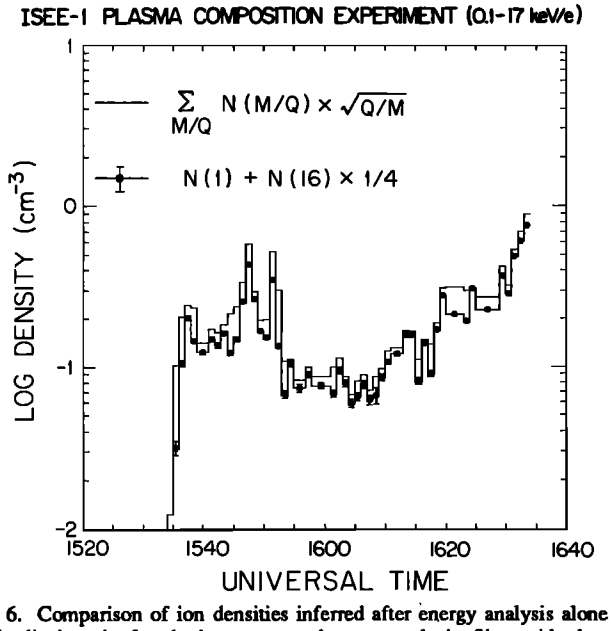

Fig. 6. Comparison of ion densities inferred after energy analysis alone (plain line) and after both energy and mass analysis (line with data points). The error bars on the latter show standard deviations due to counting statistics (about the same as or smaller in the other case). Mass analysis was limited to $M/Q=1$ (H^+) and $M/Q=16$ (O^+). Differences between the graphs suggest additional ion species.

The frequency of the EHC waves varies from 1.1 to 1.6 f_{cH}, with the average equal to ~1.25 f_{cH}. Estimates of the magnitude of the wave vector **k** can be obtained in two ways (see also *Kintner et al.* [1978]). First, the quasi-monochromatic nature of the waves suggests that Doppler shifting must be small. The half width at half maximum had an average value of $\Delta f/f \leq 0.1$. Assuming that the measured width in the peak is due to the Doppler shift, the wave vector can be calculated from

$$\Delta f = f' - f = \mathbf{k}\cdot\mathbf{v}$$

where f' is the frequency in the spacecraft frame, f is the frequency of the plasma frame, and **v** is the relative velocity between the plasma and the spacecraft. Although the complete $\mathbf{E}\times\mathbf{B}/B^2$ velocity could not be calculated during this time period, $(\mathbf{E}\times\mathbf{B})_z/B^2$ was usually less than the satellite velocity, so the spacecraft velocity was used in the calculation. The measured Δf therefore yield values of $k \approx 3$–$6\ \mathrm{km}^{-1}$. Since theories of EIC waves yield values of the wave vector comparable to the ion gyroradius, an estimate of the temperature of the ions supporting the wave can be obtained using the magnitude of the wave vector (calculated above) and

$$k\rho_i = \frac{k v_{th,i}}{\Omega_i} \sim 1,$$

where $v_{th,i}$ is the ion thermal velocity, ρ_i is the ion gyroradius, and Ω_i is the ion cyclotron frequency. The relevant hydrogen temperature T_H would be ~6–21 eV, implying the existence of a cool background ion population. Second, there were several spectra with a double-peaked structure which could be explained by Doppler shifting, assuming $\mathbf{k} \approx \mathbf{k}_\perp$, because of the geometry of the booms, magnetic field, and satellite velocity. For these events, $k \approx 2-4\ \mathrm{km}^{-1}$, and assuming $k\rho_H \sim 1$, $T_H \sim 8-30$ eV. These calculations assumed that the observed Doppler shift was not due to the velocity of the ion beams. If we assume that the shift due to the beam velocity is important, we obtain $k \sim 0.5-1.5\ \mathrm{km}^{-1}$ or T_H for the beam of 200–1000 eV. Since the magnetic field is <6° out of the ecliptic plane, $k_\parallel/k_\perp$ can be estimated from the spin modulation of the amplitude of the filter data. Sharp minima in the amplitude of the waves occurred when the booms were aligned with the magnetic field. The shape of the minima is consistent with $0.05 \leq k_\parallel/k_\perp \leq 0.2$. One of the individual burst samples also had a modulation consistent with $0.1 \leq k_\parallel/k_\perp \leq 0.2$; however, time variability in the wave amplitude could also explain the observed variation, and such modulation was not observable in other burst samples.

Because there were fewer samples near f_{cHe} and f_{cO} and because the frequencies are lower and therefore closer to the burst mode resolution, the average properties are not as well determined as for the f_{cH} case. For the samples peaked near the He^+ cyclotron frequency the average was ~1.1 f_{cHe}, with a range from 1 to 1.2 f_{cHe}. The observed half widths of the peaks were almost always within the 2-Hz resolution of the measurement. For the range of spacecraft velocities, therefore, $k \geq 3\ \mathrm{km}^{-1}$, and assuming $k\rho_{He} \sim 1$, $T_{He} > 6-170$ eV. The one spectrum with a double-peaked structure yielded $T_{He} \sim 16$ eV. For the events identified as possible electrostatic oxygen cyclotron waves, f_{cO} varied from 2.6 to 4 Hz, and the observed peak frequencies varied from 4 to 6 Hz, with the average dominant frequency approximately equal to 1.4 f_{cO} (this may not be very meaningful, since f_{cO} is so close to the 2-Hz resolution of the spectra). The half width was usually <2 Hz, yielding $T_O \geq 6-25$ eV, with the assumption that $k\rho_O \sim 1$.

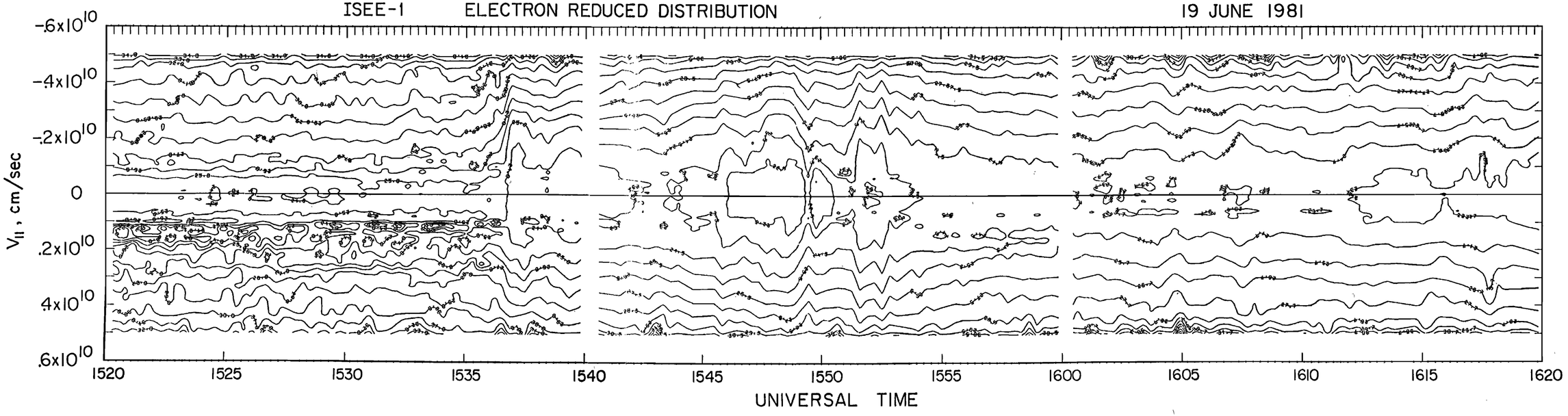

Plate 1. The reduced electron distribution function ($F(v_\parallel) = f(v_\perp, v_\parallel) 2\pi dv_\perp$ plotted versus time.

The frequency and wavelength ranges obtained for the hydrogen cyclotron waves can be compared with previous experimental results from the S3-3 satellite and with various theoretical predictions. The average frequency of the EHC waves observed by the S3-3 satellite is ~1.2 f_{cH} [*Bergmann*, 1984; M. A. Temerin, private communication, 1984]. Since the S3-3 instrument was a three-axis instrument, $k_\parallel/k_\perp$ was directly measured and found to be usually less than 0.2 [*Bergmann*, 1984]. These values are consistent with those obtained herein, which suggests that the waves at high altitudes are generated by the same mechanism as those at low altitudes. *Bergmann* [1984], using linear dispersion relations and a single ion species, concluded that the observed S3-3 wave parameters were most consistent with the current-driven instability.

Wave observations were also obtained at frequencies above 100 Hz by the University of Iowa swept frequency receiver. VLF hiss was very intense in the high-density regions and reduced in both intensity and frequency extent in the low-density regions. Figure 7 presents two representative examples of composite spectra obtained during the period of the EHC waves described above. The first spectrum (at ~1600:40) is generally smoothly falling from the peak above f_{cH} up to the region of z mode and auroral kilometric radiation (AKR). In contrast, the second (at ~1611:20) shows several emission features in the domain between f_{pH} and f_{pe}. The observed AKR in both samples was very intense.

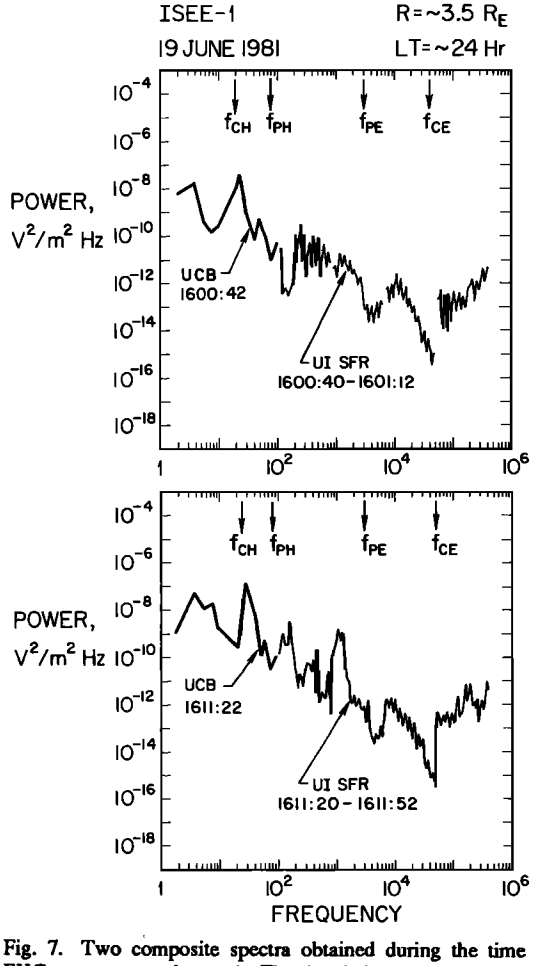

Fig. 7. Two composite spectra obtained during the time period when EHC waves were observed. The data below ~120 Hz are from the UCB burst mode; the data above ~100 Hz are from the University of Iowa swept frequency receiver (SFR). Note that there may be some time aliasing since the UCB data are obtained in 0.5 s whereas an SFR spectrum requires 32 s.

5. Sources of Free Energy

Ion beams and field-aligned currents have both been proposed to provide the free energy for growth of the electrostatic ion cyclotron waves which have been observed in the auroral zone. Comparisons of the observational data with theoretical predictions have not yet resolved the question of which is the dominant mechanism [e.g., *Kintner et al.*, 1979; *Cattell*, 1981; *Kaufmann and Kintner*, 1982, 1984; *Cattell*, 1984; *Bergmann*, 1984; *André*, 1985; *André et al.*, 1987]. This is in part due to the unmeasured portions of the ion and electron distributions and the low time resolution for current and particle measurements but also to the inescapable problem that when the waves are observed the particle distributions are likely to be marginally stable [e.g., *Kaufmann and Kintner*, 1982]. During the event described herein, both currents and beams occurred. Another free energy source, the relative streaming of O^+ and H^+ ions, can also produce waves near the ion cyclotron frequency [*Bergmann et al.*, 1988; *Kaufmann et al.*, 1986; *Roth et al.*, 1989]. The very different time resolutions of the wave measurements (0.5 s, repeated every 128 s), the current measurement (~0.25 s), and the ion measurement (~64 s) do not allow for detailed correlations between wave properties (such as amplitude, coherence, etc.) and the magnitude of the current or shape of the ion distribution function; however, the observed relationships provide information on the likely dominant generation mechanism for the measured waves.

Current-driven electrostatic ion cyclotron waves will be considered by comparing the observations described above to the linear dispersion relation and to prior theoretical studies. The first step is to examine wave and particle measurements to determine the density and temperature of various components of the plasma. These will be used with the current measurements to estimate the electron drift velocity. We will show that when waves near the cyclotron frequency were observed, the drift velocity was larger than the critical drift and that EIC waves were suppressed in regions of large field-aligned current when the density and/or temperature were large. Next, we will examine the dependence of the wave frequency on ion composition and conclude that it is consistent with current-driven EIC waves and inconsistent with the two-stream instability. Ion beam-driven modes, including the ion two-stream instability and beam-driven EIC waves with and without a current, will then be examined utilizing previous theoretical studies and numerical solutions to the linear dispersion relation calculated from the observed parameters. We will show that the ion two-stream instability is suppressed for the parameters observed during the time when waves near the cyclotron frequencies occurred. We then solve the dispersion relation, including explicitly the current, the ion beams, and the ion composition, and show that (1) the instability is due to the current, (2) the beams provide damping, and (3) there is a switch in the most unstable mode from f_{cH} to f_{cO} when n_{O^+}/n_{H^+} increases. We conclude that our observations are most consistent with the current-driven mode.

First, we will consider field-aligned currents as a source of free energy for the observed waves. The current-driven instability is actually driven by the electron drift which must be above some critical value for marginal linear instability. For example, for an equal temperature plasma (assuming Maxwellian populations) with only a single stationary ion species (hydrogen), the drift of electrons, V_D, must exceed 0.3 times the thermal drift u_e [*Kindel and Kennel*, 1971]. As the temperature ratio T_e/T_i increases, the critical drift decreases (see, for example, *Bergmann* [1984], Table 4, which shows values of $V_D/u_e \approx 0.14$ for

$T_e > T_i$ with an additional ion population). In order to determine whether the measured field-aligned currents are above the threshold for linear instability, it is necessary to know (1) whether the current is carried by drifting electrons or by a feature such as a loss cone in the electrons, (2) the electron and ion density and temperatures, and (3) whether there is more than one component for either species. The method we have used to answer these questions is to compare the total density determined by the wave cutoff (measured by the University of Iowa swept frequency receiver) and the densities measured by the particle detectors and to examine the distribution functions for evidence of current-carrying populations.

Figure 8, in which the density determined from each method is plotted, shows that most of the electron density is at energies from 0.1 to 7 keV, except during the period from ~1520 to ~1540 (when there must have been a large population of cold electrons (~0.5 to 1/cm^3)). The measured ion density is also approximately equal to the total density except before ~1540, although there is evidence for an unmeasured cold population with a density of $\lesssim$0.02/cm^2 from ~1555 to ~1610. During the period when the EHC waves were observed (~1600–~1620), the density was ~0.1–0.2/cm^3, and there was no substantial cold electron population. The field-aligned current was usually $\lesssim 2\times10^{-8}$ A/m^2, with several smaller-scale size sheets with magnitudes up to $\sim 5\times10^{-8}$ A/m^2. Assuming that the current was carried by a drifting Maxwellian with the measured density and temperature, this corresponds to $V_D/v_{the} \approx 0.07$–0.15, which is at

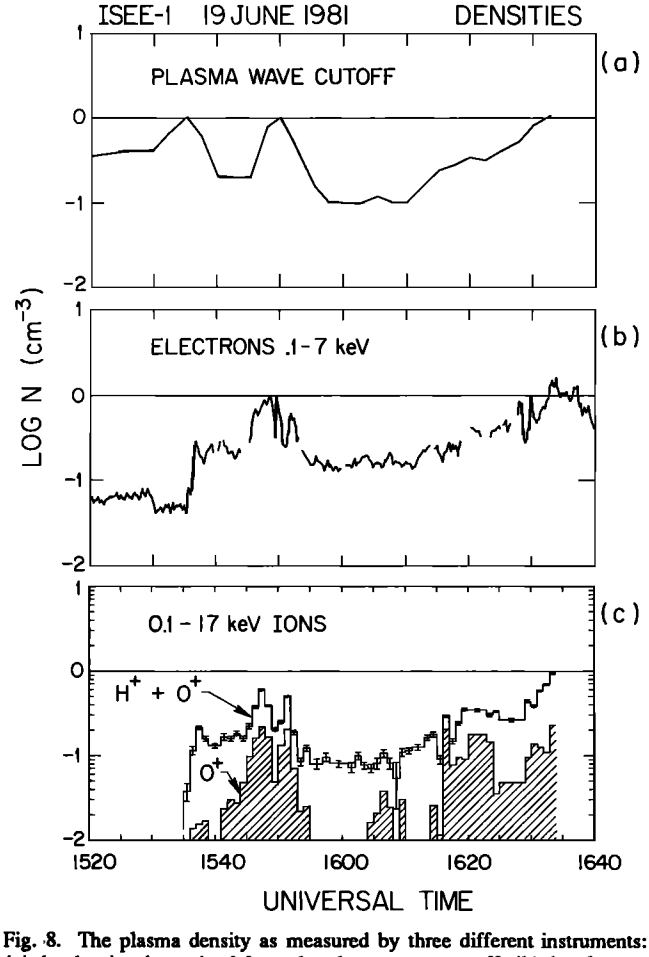

Fig. 8. The plasma density as measured by three different instruments: *(a)* the density determined from the plasma wave cutoff, *(b)* the electron density measured between 0.1 and 7 keV, and *(c)* the ion density measured between 0.1 and 17 keV for O^+ ions (hatched) and ($O^+ + H^+$) ions.

the low end of the range of critical drifts for $T_e > T_i$ with a single ion beam species present [*Bergmann*, 1984]. The observed electron distribution, however, was not a drifting Maxwellian when the EIC waves occurred. In fact, the distribution was quite variable in character, as can be seen in Plate 1, in which the reduced electron distribution ($F(v_\parallel) = \int f(v_\perp, v_\parallel) 2\pi dv_\perp$) is plotted versus time. Occasionally, there were beams at $\lesssim$1 keV. For example, during the downward current sheet at ~1552 there was a low-energy upward electron beam, and in the upward current near 1607–1609 there were downward beams. Unfortunately, an accurate calculation of the current carried by the observed electrons could not be made due to the loss of one detector.

To lend credence to the idea that the waves are current-driven, it is important to understand why EIC waves were not observed in other (often larger) regions of current. For example, one of the largest current densities, at 1536, was flowing into the ionosphere with no simultaneous ion beams. Figure 8 implies that at that time there was a large cold electron population which must have carried the current since the observed hot electrons were almost entirely downgoing. Assuming a temperature of 1–10 eV for the cold electron population with the inferred density of 0.9/cm^3, $V_D/v_{the} \approx 0.003$–$0.01$ which is much less than the critical value for instability with $T_e = T_i$. There was not a burst sample at this time, but examination of both the University of California at Berkeley and the University of Iowa filters showed no evidence for a peak at or slightly above the hydrogen cyclotron frequency. At ~1543 a large upward current occurred in a region of only hot electrons (if the measured electrons were a drifting Maxwellian, then $V_D/v_{the} = 0.1$) and upflowing ion beams. The burst sample during that current had wave power near f_{cH} but no coherent waves. The largest current during this period ($j \sim 37\times10^{-8}$ A/m^2 at ~1632) was also in the region with the highest density ($n \gtrsim 1$/cm^3) and electron temperature and therefore the lowest value of V_D/v_{the}. This observation, that EIC waves were suppressed in regions of large current when the corresponding value of V_D/v_{the} was small, is consistent with theories of current-driven EIC waves.

A second indication that the waves may be current-driven is the dependence of the wave frequencies on the ion composition. *Kindel and Kennel* [1971] showed that for the current-driven instability, H^+ cyclotron waves are linearly more unstable until the density ratio $O^+/(H^+ + O^+)$ exceeds ~10–15%, when O^+ cyclotron waves become linearly more unstable. The observations presented herein (compare the frequency at which the peak power occurred (Figure 5) with the composition in Figure 6) are consistent with this. When the density ratio was $\lesssim$10%, only EHC waves were observed; from ~10 to 20%, EHC and waves near f_{cHe} and f_{cO} occurred. This dependence of frequency on composition is opposite to that obtained for the ion two-stream instability. As shown in *Bergmann et al.* [1988], the most unstable oblique mode is above f_{cH} when the percentage of O^+ is high and decreases to below f_{cH} when there is less O^+. More detailed comparisons with the ion two-stream instability will be described below.

There are also theories which predict the occurrence of EIC waves in a system with a subcritical electron drift (*Tetreault*, 1991). The EIC waves, in this case, are part of the process by which ion holes evolve into double layers and subsequently decay. No comparisons with this model will be made herein.

Next, we compare the observations quantitatively using a linear dispersion relation solver containing ion beams including composition and either drifting or nondrifting electrons. A car-

toon representation of the particle distributions included is shown in Figure 9. In the presence of two drifting ion populations with a relative drift $\Delta V = V_H - V_O$, the strongest instability can occur when two eigenmodes have a similar dispersion in $\omega - k$ space. In our case the strongest possible candidate for instability occurs for parallel propagation when the slow hydrogen beam acoustic mode with an approximate dispersion relation $\omega \sim k\,(V_H - c_H)$ couples with a fast oxygen beam acoustic mode $\omega \sim k\,(V_O + c_O)$, where $c_j^2 = (n_j/n_e)(T_e/m_j)$ are the density weighted sound speeds of species j. The conditions for this interaction are (condition 1)

$$\Delta V/u_e < (1+\delta)(\omega_H/\omega_e)[1+(\omega_O/\omega_{lH}\delta)^2]^{1/2}$$

[*Bergmann et al.*, 1988] and (condition 2) $V_j > u_j$ [*Roth et al.*, 1989], where u_j are the thermal spreads, ω_j are the plasma frequencies, and $\delta = [(n_H/n_O)(m_H/m_O]^{-1/3}$. Condition (1) assures that the drift velocities are close enough together that the slow H^+ and fast O^+ modes can acquire similar phase velocities to enable a fluidlike interaction. Condition (2) assures that the phase velocity of each mode is approximately constant; the contribution of finite ion temperatures modifies each eigenmode dispersion due to additional terms in the expansion of the plasma Z function. For a sufficiently large ion thermal spread the phase velocities of the acoustic modes cannot overlap, and this interaction is stabilized.

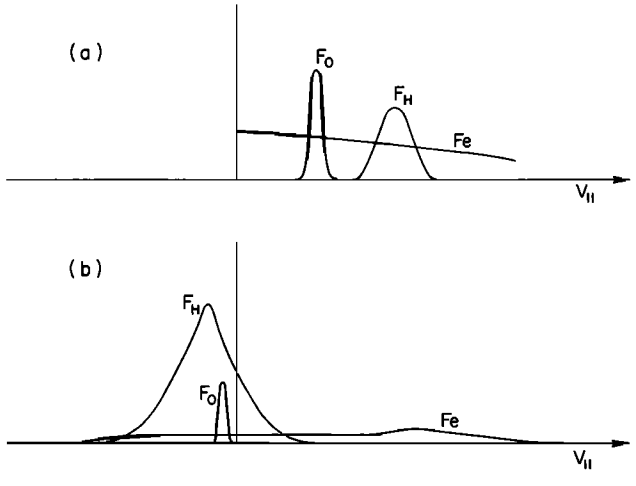

Fig. 9. Schematic representation of the distributions considered in the numerical study of the dispersion relation: *(a)* without electron drift and *(b)* with electron drift.

For our benchmark set of parameters, $V_H/u_e \sim 0.03$, $V_H/V_O \sim 2$, condition 1 is well satisfied for all ranges of n_O/n_H values. Figure 10 shows the maximum growth rate as obtained from the solution of the dispersion relation for the above parameters with $n_H = n_O$, $V_O/u_O = 5$, and varying the ratio of V_H/u_H. It can be seen that around $V_H/u_H \sim 2.3$ the parallel ion-ion instability is quenched, with a growth rate $< 3 \times 10^{-4}\ \omega_H$. The observed contours of hydrogen show relatively warm distributions, and we conclude that the heated hydrogen population is able to quench the parallel ion-ion instability.

The relative drift between each ion species and the electrons can also excite kinetic drift acoustic waves. The growth rate is proportional to the imaginary part of the dielectric function

$$\mathrm{Im}\,\varepsilon \propto \frac{\omega_H^2}{k^2 u_H^2}\,\frac{\omega - kV_H}{k\,u_H}\,e^{-(\omega - kV_H)^2/k^2 u_H^2} + \frac{\omega_e^2}{k^2 u_e^2}\,\frac{\omega}{k\,u_e}\,e^{-(\omega/k\,u_e)^2} \quad (1)$$

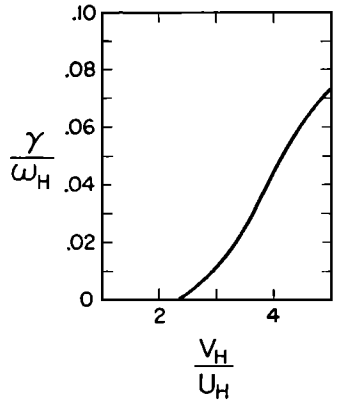

Fig. 10. Plot of the maximum growth rate for the parallel ion two-stream instability versus $V_H = u_H$, the hydrogen drift/thermal speed for $n_H = n_O$, $V_H/u_e = 0.03$, $V_H/V_O = 2$, and $V_O/u_O = 5$.

with a similar expression for the oxygen ions. However, for our parameters the exponent of the electron term in (1) is very small, the damping from the electron term is larger than the ion inverse damping, and the parallel modes which may be excited by ion beams are stable. In our parameter regime where the cold parallel modes could satisfy the instability condition, they dominate the oblique modes [*Bergmann et al.*, 1988]. Quenching of these ion-ion modes also quenches the oblique modes. The kinetic oblique modes are also damped by the electrons. Therefore we will focus on oblique wave excitation due to a nonthermal electron distribution function.

The observed electrons have a nonzero first moment of the distribution function. Because of the insufficient details on the electron distribution function we shall model them as drifting Maxwellians. It was shown by *Kindel and Kennel* [1971] that the threshold for the oblique ion cyclotron modes is below the parallel acoustic modes which are excited by the electron current.

Figure 11 shows the lowest dispersion curves above the hydrogen gyrofrequency around the largest growth rates for two ion density ratios, $n_O/n_e = 0.1$ and 0.5. In Figure 11 the propagation angle is 83°, $T_e/T_H = 3.5$, $u_H/u_O = 3$, $\Omega_H/\omega_H = 0.24$, $V_e/u_e = 0.16$, $|V_H/u_H| = 2.1$, and $|V_O/u_O| = 3.1$ ($V_H, V_O < 0$). For the given parameters the maximum growth rate is $\gamma/\omega_H = 0.0041$ (0.0021) at $\omega = 1.1$ (1.0), and $k\rho_H \cong 1.05$ for $n_O/n_e = 0.1$ (0.5), respectively. In the vicinity of the hydrogen gyrofrequency the approximate dispersion relation may be obtained by keeping only the first cyclotron term in the hydrogen Bessel summation and the leading terms in the oxygen and electron susceptibilities. The dispersion relation becomes $\omega - kv_H = \Omega_H/(1-\alpha(\omega,k))$ where $\alpha = O[\Gamma_1(k^2\rho_H^2)]$ includes all the nonresonant corrections. Since $V_e/u_e << 1$, we may neglect the electron plasma function contribution which results in

$$\omega \cong -k_{||}\,|V_H| + \quad (2)$$

$$\Omega_H\{1 + \Gamma_1(k_\perp^2\,\rho_H^2)/[1 + k^2\lambda_H^2 + \frac{n_e}{n_H}\,\frac{T_H}{T_e} + \frac{n_O}{n_H}\,\frac{T_H}{T_O}]\}$$

which is a Doppler-shifted electrostatic hydrogen cyclotron mode with oxygen corrections. Here $\Gamma(x) = e^{-x}\,I(x)$ where I is the modified Bessel function. The resonant oxygen contribution to the hydrogen cyclotron term is proportional to

$$\Gamma_{16}(k_\perp^2\,u_O^2/2\Omega_O^2)\,Z\,(\omega - 16\,\Omega_O - k_{||}\,V_O/k_{||}\,u_O)$$

which is negligibly small. One observes from (2) that addition

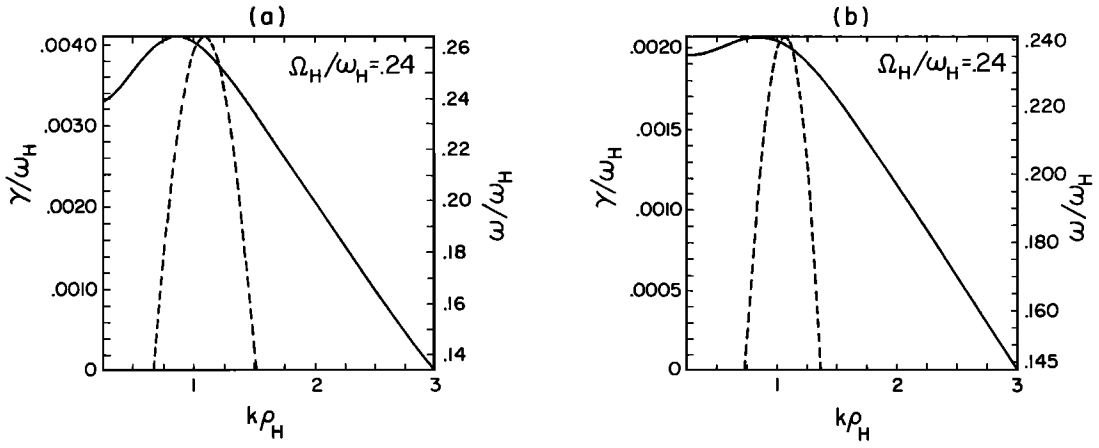

Figure 11. The dispersion curves for growth rate and real frequency near Ω_H for *(a)* $n_O/n_e=0.1$, and *(b)* $n_O/n_e=0.5$, for $\theta=83°$, $T_e/T_H=3.5$, $u_H/u_O=3$, $V_e/u_e=0.24$, $V_H/u_H=-2.1$, and $V_O/u_O=-3.1$. The real frequency curve is the same for both cases, on this scale.

of oxygen density decreases slightly the eigenfrequency of the hydrogen cyclotron mode. This brings the frequency closer to the hydrogen gyrofrequency, increasing the damping of the waves, since the growth rate is proportional to

$$\frac{2\omega_e^2}{k^2u_e^2}\frac{\omega-k_\parallel V_e}{k_\parallel u_e}Z_I\left[\frac{\omega-k_\parallel V_e}{k_\parallel u_e}\right]+ \sum_s\frac{2\omega_s^2}{k^2u_s^2}\frac{\omega+k_\parallel V_s}{k_\parallel u_s}\sum_n\Gamma_n Z_I\left[\frac{\omega-n\Omega_s+k_\parallel V_s}{k_\parallel u_s}\right] \quad (3)$$

where the summation is over the ions and $Z_I(x)\sim e^{-x^2}$ denotes the imaginary part of the plasma function. Therefore the addition of oxygen makes the hydrogen cyclotron mode more stable, and for a marginally stable interaction an enhanced oxygen flux may stabilize the interaction. For the given parameters, decreasing the electron drift to $V_e/u_e=0.12$ stabilizes the high-density case (condition 2) while the low-density case is still unstable. This may explain the absence of observed wave power above the hydrogen cyclotron frequency when the oxygen density is enhanced. Addition of cold nondrifting ion population does not affect this instability.

In the low-frequency range the unstable interaction is also due to the destabilizing effect of electrons and damping by the ions. Around the oxygen gyrofrequency the hydrogen ions are not resonant and do not affect the real frequency. The dispersion relation is obtained similarly to equation (2) and is given in the oxygen frame by

$$\omega\cong\Omega_o\{1+\Gamma_1(k_\perp^2\rho_O^2)/[1+k^2\lambda_O^2+\frac{n_H}{n_O}\frac{T_O}{T_H}+\frac{n_e}{n_O}\frac{T_O}{T_e}]\} \quad (4)$$

showing that an increase in n_O moves the frequency away from the oxygen gyrofrequency, decreasing the damping. Therefore, close to marginal stability an increase (decrease) in the oxygen density makes the growth rate positive (negative). This behavior is in contrast to that at the higher hydrogen cyclotron frequency. Figure 12 shows the real frequencies and the growth rates in the oxygen reference frame for $V_e/u_e=0.16$, $|V_H/u_H|=1.3$, and $\Omega_H/\omega_H=0.24$ ($\Omega_O/\omega_H=0.015$) at the propagation angle 88° which maximizes the growth rate. The maximum growth rates are $4\times10^{-4}\ \omega_H$ and $1.2\times10^{-4}\ \omega_H$ at $\omega/\Omega_O\cong1.3$ and 1.15, and $k\rho_O=0.9$ for $n_O/n_e=0.5$, 0.1, respectively. Enhanced density of oxygen decreases (quenches) the modes above the hydrogen gyrofrequency and increases (excites) the modes above the oxygen gyrofrequency.

6. EFFECT OF THE WAVES ON THE IONS

With the assumption that the observed O^+ and H^+ beams were accelerated through the same potential drop, the interaction between the ion species and waves at and below the spacecraft can be addressed. Ion beams of all species would have the same peak energy per charge, and each would have the temperature of its source population. Any differences from such distributions can be attributed to interactions between the various ion species and/or interactions with waves due to other free energy sources. Both theoretical and experimental studies of O^+, He^+, and H^+ ion beams have been made utilizing this assumption by numerous authors [e.g., *Collin et al.*, 1981, 1987; *Bergmann and Lotko*, 1986; *Kaufmann et al.*, 1986; *Reiff et al.*, 1986, 1988; *Dusenbery et al.*, 1988; *Roth et al.*, 1989; *Winglee et al.*, 1989]. These studies have all shown that the ions are strongly heated and that often there is a transfer of energy from the H^+ ions to the O^+ ions which may be dependent on the composition ratio [see *Collin et al.*, 1987; *Reiff et al.*, 1988]. The studies of *Reiff et al.* [1988] and *Collin et al.* [1987] suggested that during solar maximum, O^+ and H^+ have comparable energies in contrast to solar minimum when the O^+ is more energetic. Their explanation was that the O^+-H^+ relative streaming instability was most efficient at transferring energy to the O^+ ions when the O^+/H^+ ratio was low, as occurs on a statistical basis during solar minimum. Note that the event described herein occurred at solar maximum.

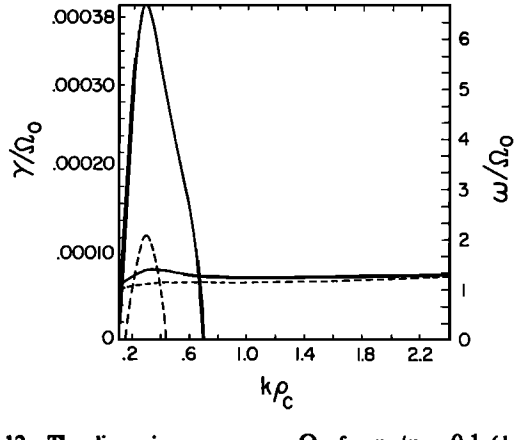

Fig. 12. The dispersion curves near Ω_O for $n_O/n_e=0.1$ (dashed line) and $n_O/n_e=0.5$ (solid line).

Distribution functions for O^+ and H^+ are presented in Figure 13 for that portion of the event when waves near the various cyclotron frequencies occurred. The time indicated is at the end of the sample, and the velocities are scaled so that O^+ and H^+ ions with the same energy would occur at the same distance from the center. For most of the time periods shown, there were distinct O^+ beams, whereas the H^+ beams were often obscured by a nearly isotropic component, which may have originated above the spacecraft (compare bottom panels in Figure 1). When both O^+ and H^+ beams are distinct in these contour plots, for instance at 1602:22, 1605:34, 1607:42, and 1618:21, the O^+ beams are generally more energetic. This may not seem to agree with the statistical results for data during solar maximum, but this event does not have O^+/H^+ ratios as high as are typically found then, at least not according to Figure 8. This figure is not directly comparable to the results of *Collin et al.* [1987] and *Reiff et al.* [1988], however, since those were obtained with an isotropic component subtracted. We have tried to emulate that by comparing the energies at peak upward flux of O^+ and H^+ ions as a function of the ratio of the same two fluxes (not shown), but the ~40 data points available have too much scatter to show a clear trend. The data of *Collin et al.* [1987] also show large scatter, and it is only on a much larger statistical basis that their argument holds.

There is evidence in the distributions for the operation of both the O^+-H^+ two-stream instability and the EIC waves. The tendency of the O^+ beams to have a higher energy than the H^+ beams and the fact that V_H was not 4 times larger than V_o are consistent with the two-stream instability. This occurred throughout most of the time period and provides evidence that the two-stream instability modified the distributions below the satellite at altitudes where that mode was unstable. The broadening of the O^+ distributions during periods when waves near f_{cHe} and f_{cO} occurred but not during periods of waves near f_{cH} is consistent with heating by the locally observed EIC waves. Several specific examples can be seen in Figure 14 which presents O^+ and H^+ distributions and simultaneous power spectra. The spectrum in Figure 14*(a)* has a peak slightly above

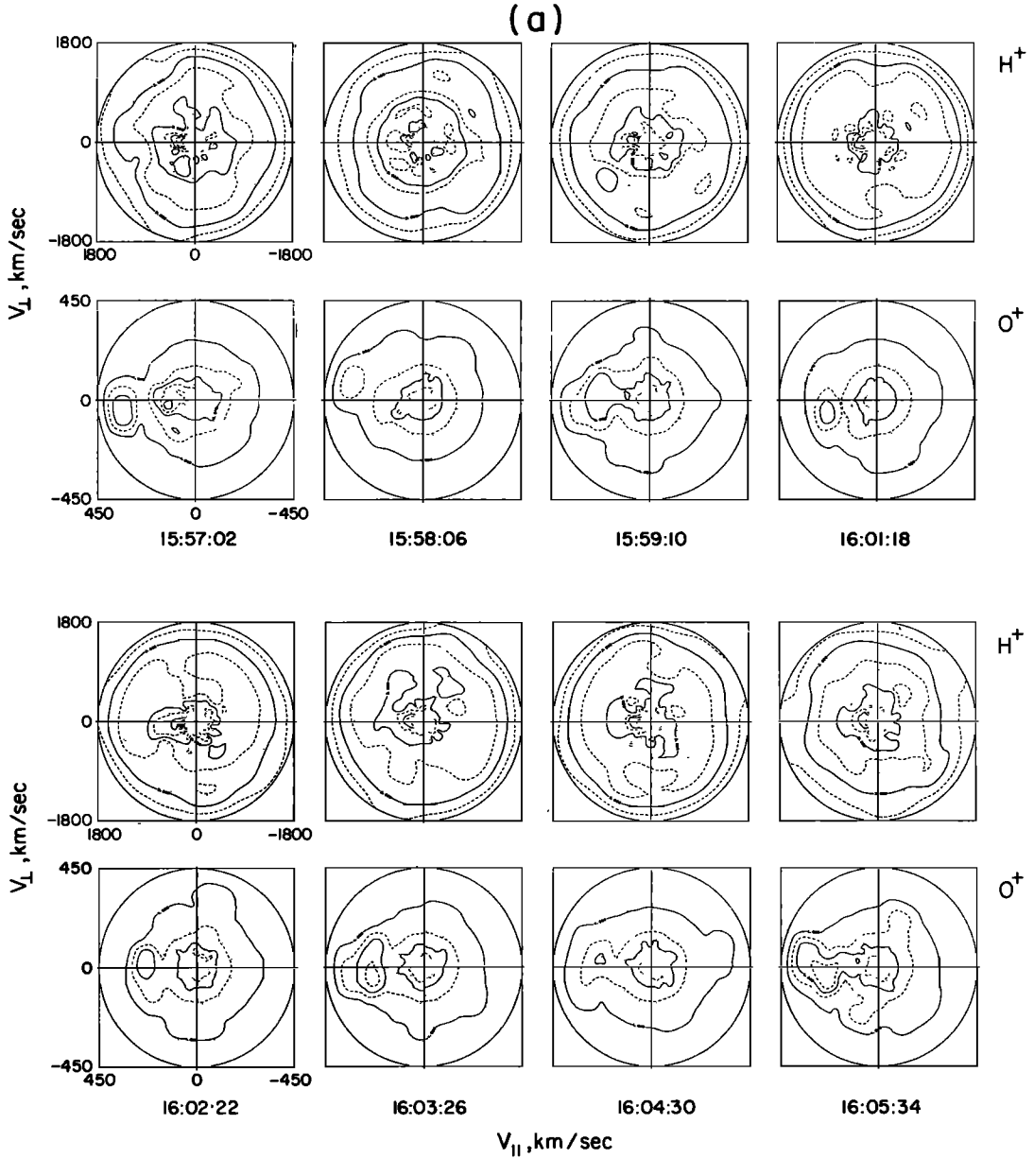

Fig. 13. The distribution function ($f(v_\perp, v_\parallel)$) for H^+ and O^+ for the time period when EIC waves were observed.

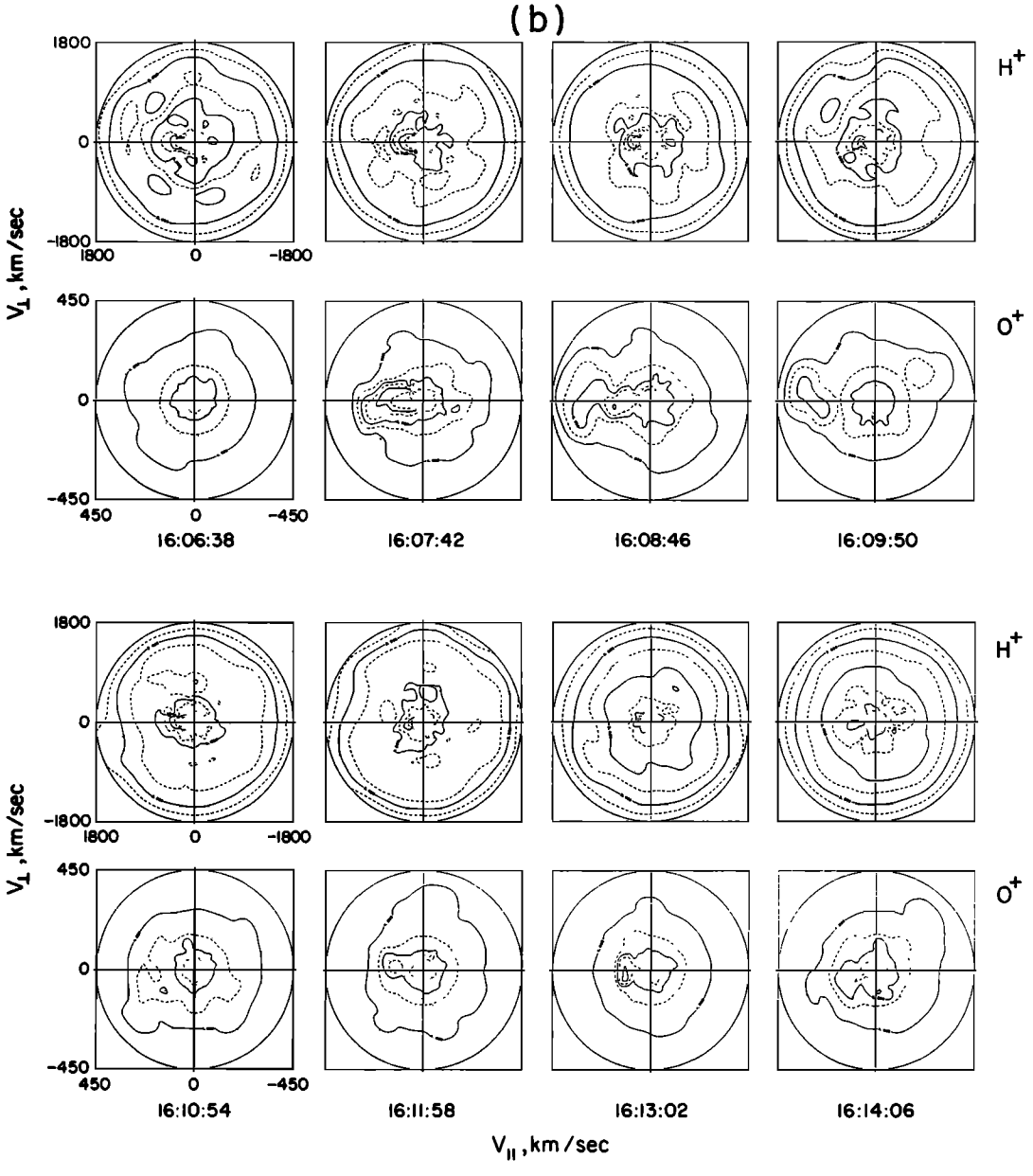

Fig. 13. (continued)

f_{cH}. The H^+ distribution shows strong perpendicular heating, while the O^+ beam retains beamlike characteristics. The spectrum in Figure 14*(b)* has power near both f_{cH} and f_{cHe}, and in this case both distributions show strong heating and modification from a beamlike distribution. The spectrum in Figure 14*(c)* had a peak at ~2.8 f_{cH}. These were the most intense waves observed during the event. Both O^+ and H^+ were upflowing, and both show evidence of strong modification. During the period of the spectrum in Figure 14(*d*) which peaked near f_{cO}, the O^+ distribution shows heating of the background ions at ~90° as well as perpendicular heating of the beam.

7. Discussion and Conclusions

The low-frequency electric field data presented herein have provided evidence for the existence of electrostatic hydrogen cyclotron waves on auroral field lines at altitudes of ~2.5–~4 R_E. The identification of the observed waves near the cyclotron frequencies as electrostatic ion cyclotron waves is based on the consistency of the observed and deduced properties of the waves with theories of EIC waves. Neither magnetic measurements nor density measurements at the relevant frequencies were available to provide the definitive proof that the waves were electrostatic. The S3-3 satellite did have density fluctuation measurements and did show that the waves observed in the electric field were electrostatic. The average frequency and propagation angle are within the range observed by the S3-3 satellite at lower altitudes. In addition, the waves have the same association with regions of low density, ion beams, and field-aligned currents as was observed at lower altitudes. This implies that the cyclotron frequency waves observed by ISEE were also EHC waves and that the waves are excited by the same free energy source throughout the altitude range ~1.5–4 R_E. Studies based on the S3-3 data were not able to definitively determine the excitation mechanism. The fact that all the identified EHC

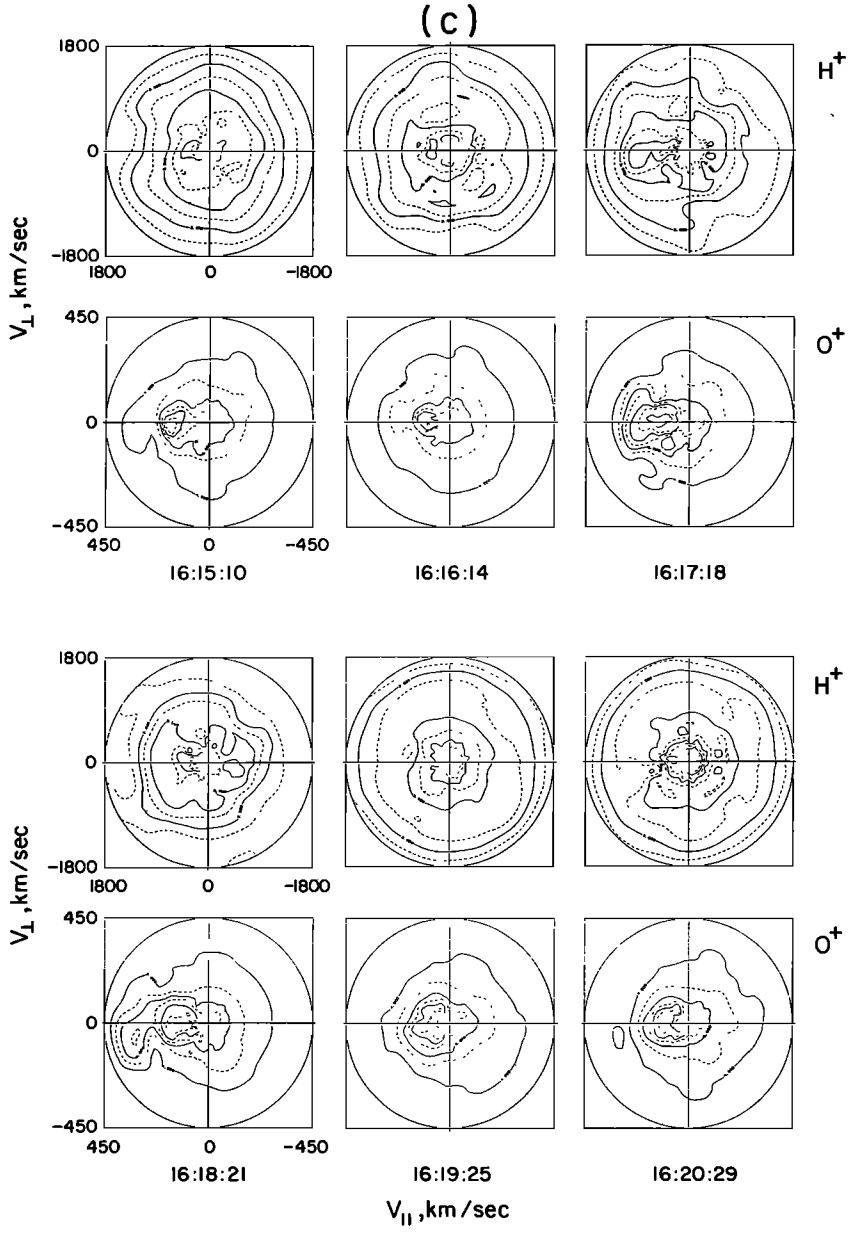

Fig. 13. (continued)

wave events occurred when there were ion beams [*Kintner et al.*, 1979] and a careful numerical study of the linear dispersion relation for one particular event [*Kaufmann and Kintner*, 1982, 1984] both pointed to ion beams as the most likely free energy source. A linear study of both current- and beam-driven modes based on the average range of observed plasma parameters for S3-3, however, concluded that the observed wave properties were more consistent with current-driven modes [*Bergmann*, 1984]. Researchers were hampered in their efforts by the lack of information on the cold plasma, poor time resolution in the field-aligned current measurements, and the difficulty involved in properly including all the ion species.

For the event described herein the most complete data set yet assembled has been utilized to address the question of the instability mechanism for the waves at the ion cyclotron frequency. Good estimates of the cold electron and ion densities, ion composition ratios, high-resolution current measurements, electron distributions, and distributions of both hydrogen and oxygen ions were available. During the period when waves near the gyrofrequencies of H^+, O^+, and He^+ occurred, the available data strongly support the idea that there were no unmeasured cold ions or electrons. The ratio of $n(O^+)/n(H^+)$ varied from ~0 to 1, and there was indirect evidence for the existence of He^+. There were at least four possible sources of free energy for wave growth: (1) field-aligned currents, (2) O^+ beams, (3) H^+ beams, and (4) the relative streaming of the O^+ and H^+. The first three could drive EIC waves, while the fourth could drive the ion two-stream instability which has a similar frequency regime. Qualitative comparisons between the wave characteristics, plasma parameters, and previously published linear theories of EIC waves and two stream instabilities suggest that the observed waves near f_{cH} are current-driven EHC waves. The relationship of the dominant wave frequency to the composition ratio also lends credence to the idea that the waves near f_{cO} and

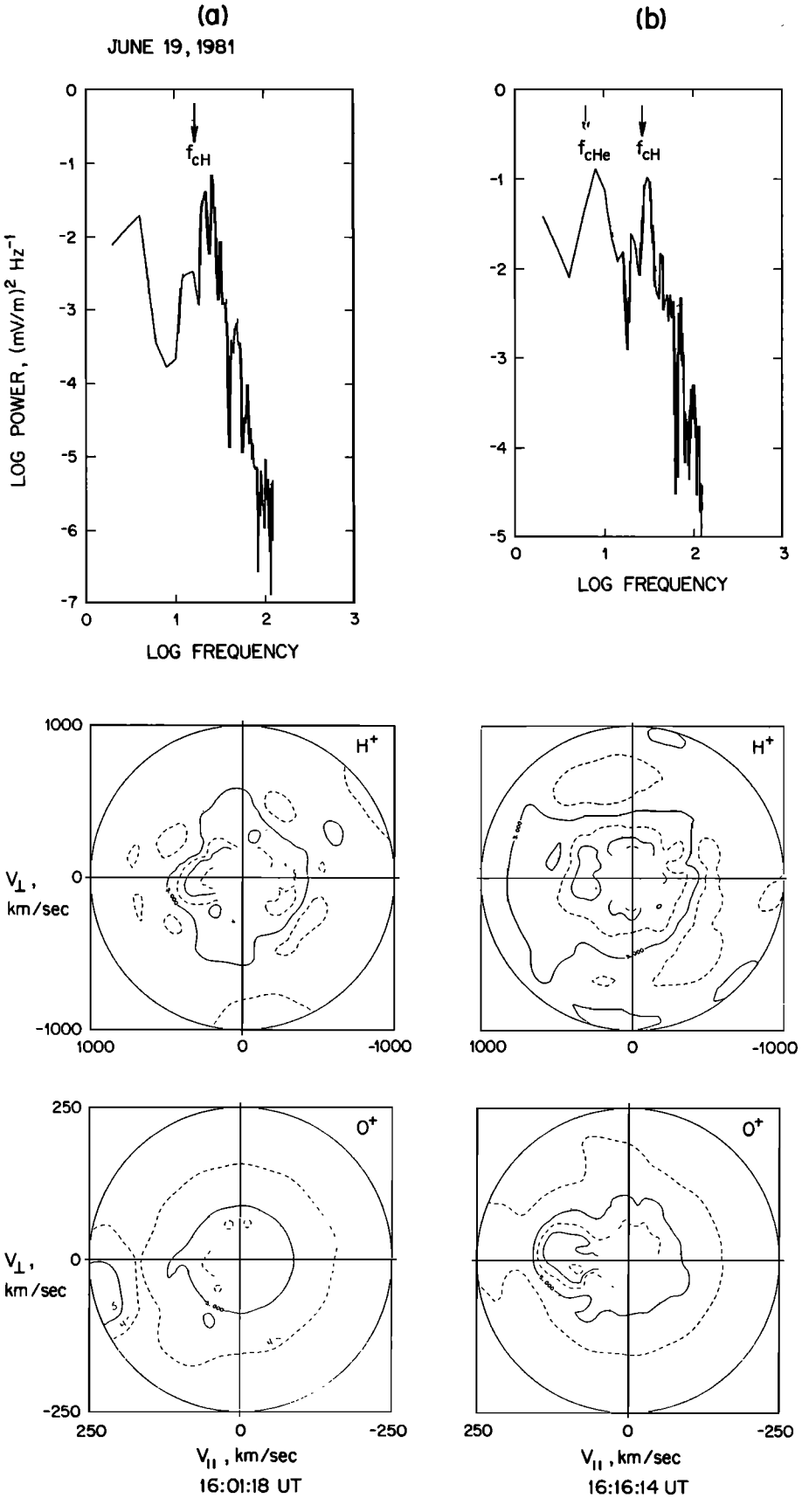

Fig. 14. Four representative examples of the electric field power spectrum and simultaneous ion distribution functions.

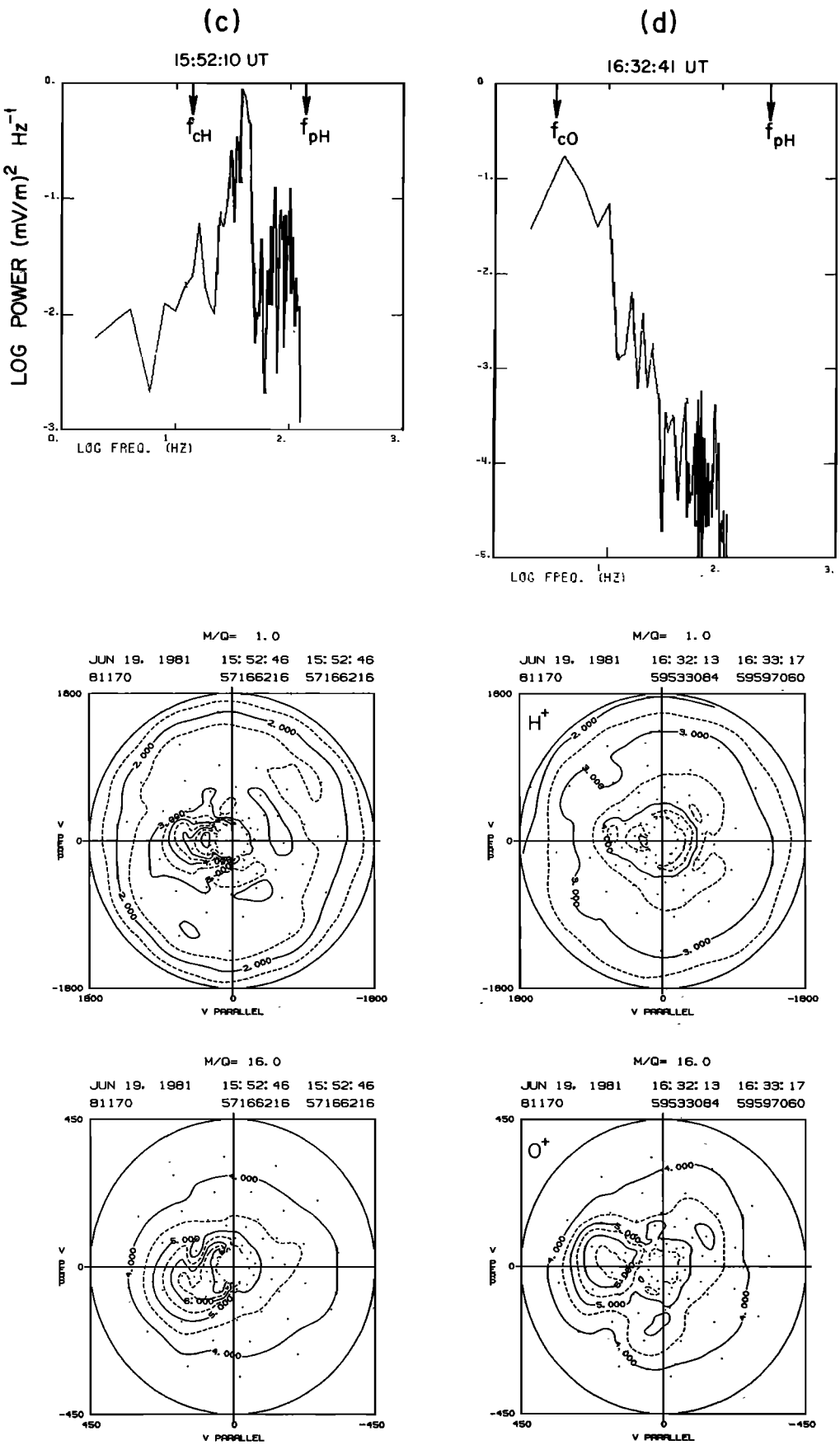

Fig. 14. (continued)

f_{cHe} are also current-driven EIC waves. Although the observed electron distributions were not drifting Maxwellians as is assumed in standard theoretical studies, there is evidence that the distribution has a nonzero first moment as required for current-driven waves.

Solutions to the linear dispersion relation have also been obtained utilizing the observed plasma parameters to determine whether the ion two-stream instability should be unstable, whether the beams or the current drive the EIC waves, and what the expected relative growth rates are. These studies have shown that the parallel ion two-stream instability is quenched by the observed warm hydrogen distributions. In addition, the parallel modes driven by an ion beam either on the electrons or on background ions are also stable. Since for our parameter regime, parallel propagating waves are more unstable than oblique ones, neither type of instability can explain the observations. Oblique modes driven by the electron current are unstable and have frequencies comparable to those observed.

Examination of the O^+ and H^+ distributions provides evidence that the ion distributions have been strongly modified at altitudes below the spacecraft. In particular, several examples of an O^+ beam having higher energy than the accompanying H^+ beam suggest a transfer of energy from the H^+ to the O^+, as expected from the ion two-stream instability. There is also evidence of further heating of the ions by the locally excited EIC waves.

Acknowledgments. We thank C. T. Russell for providing the ISEE 1 and 2 magnetometer data, D. A. Gurnett for providing the ISEE 1 plasma wave SFR and filter data, and K. Ogilvie and R. Fitzenreiter for providing the ISEE 1 electron moments and distributions. We thank R. Bergmann, W. Peterson, and M. K. Hudson for useful discussions. We also thank the two referees for useful comments. The work was supported by NASA grants NAG5-375 and NAG5-1098 at the University of California at Berkeley, NAG5-1067 at the University of California at Los Angeles, and NAG5-1093 at the University of Iowa, and by NASA contracts NAS5-28702 and NAS5-33047 at LPARL.

The editor thanks E. A. Bering and W. A. Scales for their assistance in evaluating this paper.

REFERENCES

André, M., Ion waves generated by streaming particles, *Ann. Geophys., Ser. A, 3*, 73, 1985.

André, M., H. Koskinen, G. Gustafsson, and R. Lundin, Ion waves and upgoing ion beams observed by Viking, *Geophys. Res. Lett., 14*, 463, 1987.

Ashour-Abdalla, M., and H. Okuda, Turbulent heating of heavy ions on auroral field lines, *J. Geophys. Res., 89*, 2235, 1984.

Ashour-Abdalla, M., and R. M. Thorne, Toward a unified view of diffuse auroral precipitation, *J. Geophys. Res., 83*, 4775, 1978.

Ashour-Abdalla, M., H. Okuda, and C. Z. Cheng, Acceleration of heavy ions on auroral field lines, *Geophys. Res. Lett., 8*, 795, 1981.

Bergmann, R., Electrostatic ion (hydrogen) cyclotron and ion acoustic wave instabilities in regions of upward field-aligned current and upward ion beams, *J. Geophys. Res., 89*, 953, 1984.

Bergmann, R., Three-wave coupling coefficients in a drifting bi-Maxwellian plasma, *J. Plasma Phys., 36*, 97, 1986.

Bergmann, R., and W. Lotko, Transition to unstable ion flow in parallel electric fields, *J. Geophys. Res., 91*, 7033, 1986.

Bergmann, R., I. Roth, and M. K. Hudson, Linear stability of the H^+-O^+ two-stream interaction in a magnetized plasma, *J. Geophys. Res., 93*, 4005, 1988.

Bering, E. A., The plasma wave environment of an auroral arc: Electrostatic ion cyclotron waves in the diffuse aurora, *J. Geophys. Res., 89*, 1635, 1984.

Bering, E. A., M. C. Kelley, and F. S. Mozer, Observations of an intense field-aligned ion flow and associated intense narrow band electric field oscillations, *J. Geophys. Res., 80*, 4612, 1975.

Böhmer, H., J. P. Hauck, and N. Rynn, Ion-beam excitation of electrostatic ion-cyclotron waves, *Phys. Fluids, 19*, 340, 1976.

Cattell, C. A., The relationship of field-aligned currents to electrostatic ion cyclotron waves, *J. Geophys. Res., 86*, 3641, 1981.

Cattell, C., The association of field-aligned currents with small-scale auroral phenomena, in *Magnetospheric Currents, Geophys. Monogr. Ser.*, vol. 28, edited by T. Potemra, p. 243, AGU, Washington, D. C., 1984.

Collin, H. L., R. D. Sharp, E. G. Shelley, and R. G. Johnson, Some general characteristics of upflowing ion beams over the auroral zone and their relationship to auroral electrons, *J. Geophys. Res., 86*, 6820, 1981.

Collin, H. L., W. K. Peterson, and E. G. Shelley, Solar cycle variation of some mass dependent characteristics of upflowing beams of terrestrial ions, *J. Geophys. Res., 92*, 4757, 1987.

Dusenbery, P. B., and L. R. Lyons, Generation of ion-conic distribution by upgoing ionospheric electrons, *J. Geophys. Res., 86*, 7627, 1981.

Dusenbery, P. B., R. F. Martin, Jr., and R. M. Winglee, Ion-ion waves in the auroral region: Wave excitation and ion heating, *J. Geophys. Res., 93*, 5655, 1988.

Gurnett, D. A., F. L. Scarf, R. W. Fredricks, and E. J. Smith, The ISEE-1 and ISEE-2 plasma wave investigation, *IEEE Trans. Geosci. Electron., GE-16*, 225, 1978.

Hauck, J. P., H. Böhmer, N. Rynn, and G. Benford, Ion beam excitation of ion-cyclotron waves and ion heating in plasmas with drifting electrons, *J. Plasma Phys., 19*, 253, 1978.

Hudson, M. K., R. L. Lysak, and F. S. Mozer, Magnetic field-aligned potential drops due to electrostatic ion cyclotron turbulence, *Geophys. Res. Lett., 5*, 143, 1978.

Kaufmann, R. L., and P. M. Kintner, Upgoing ion beams, 1, Microscopic analysis, *J. Geophys. Res., 87*, 10,487, 1982.

Kaufmann, R. L., and P. M. Kintner, Upgoing ion beams, 2, Fluid analysis and magnetosphere-ionosphere coupling, *J. Geophys. Res., 89*, 2195, 1984.

Kaufmann, R. L., G. R. Ludlow, H. L. Collin, W. K. Peterson, and J. L. Burch, Interaction of auroral H^+ and O^+ beams, *J. Geophys. Res., 91*, 10,080, 1986.

Kelley, M. C., E. A. Bering, and F. S. Mozer, Evidence that the electrostatic ion cyclotron instability is saturated by ion heating, *Phys. Fluids, 18*, 1950, 1975.

Kindel, J. M., and C. F. Kennel, Topside current instabilities, *J. Geophys. Res., 76*, 3055, 1971.

Kintner, P. M., On the distinction between electrostatic ion cyclotron waves and ion cyclotron harmonic waves, *Geophys. Res. Lett., 7*, 585, 1980.

Kintner, P. M., M. C. Kelley, and F. S. Mozer, Electrostatic hydrogen cyclotron waves near one earth radius altitude in the polar magnetosphere, *Geophys. Res. Lett., 5*, 139, 1978.

Kintner, P. M., M. C. Kelley, R. D. Sharp, A. G. Ghielmetti, M. Temerin, C. A. Cattell, and P. Mizera, Simultaneous observations of energetic (keV) upstreaming ions and EHC waves, *J. Geophys. Res., 84*, 7201, 1979.

Kintner, P. M., D. M. Kumpar, and E. G. Shelley, Examples of low frequency waves and energetic ions observed from DE-A, *Eos Trans. AGU, 64*, 811, 1983.

Kintner, P. M., W. Scales, J. Vago, R. Arnoldy, G. Garbe, and T. Moore, Simultaneous observations of electrostatic oxygen cyclotron waves and ion conics, *Geophys. Res. Lett., 16*, 739, 1989.

Lysak, R. L., and M. A. Temerin, Generation of Alfvén-ion cyclotron waves on auroral field lines in the presence of heavy ions, *Geophys. Res. Lett., 10*, 643, 1983.

Lysak, R. L., M. K. Hudson, and M. Temerin, Ion heating by strong electrostatic ion cyclotron turbulence, *J. Geophys. Res., 85*, 678, 1980.

Miura, A., H. Okuda, and M. Ashour-Abdalla, Ion beam driven, electrostatic ion cyclotron waves, *Geophys. Res. Lett., 10*, 353, 1983.

Mizera, P. F., et al., The aurora inferred from S3-3 particles and fields, *J. Geophys. Res., 86*, 2329, 1981.

Mozer, F. S., R. B. Torbert, U. V. Fähleson, C.-G. Fälthammar, A. Gonfalone, and A. Pedersen, Measurements of quasistatic and low frequency electric fields with spherical double probes on the ISEE-1 spacecraft, *IEEE Trans. Geosci. Electron., GE-16*, 258, 1978.

Mozer, F. S., C. A. Cattell, M. Temerin, R. B. Torbert, S. Von Glinski, M. Woldorff, and J. Wygant, The dc and ac electric field, plasma density and temperature, and field-aligned current experiments on S3-3, *J. Geophys. Res., 84*, 5875, 1979.

Mozer, F. S., C. A. Cattell, M. K. Hudson, R. L. Lysak, M. Temerin, and R. B. Torbert, Satellite measurements and theories of low altitude auroral particle acceleration, *Space Sci. Rev., 27*, 155, 1980.

Mozer, F. S., E. W. Hones, Jr., and J. Birn, Comparison of spherical double probe electric field measurements with plasma bulk flows in plasmas having densities less than 1 cm^{-3}, *Geophys. Res. Lett., 10*, 737, 1983.

Ogilvie, K. W., J. D. Scudder, and H. Doong, The electron spectrometer experiment on ISEE-1, *IEEE Trans. Geosci. Electron., GE-16*, 261, 1978.

Pedersen, A., C.-G. Fälthammar, V. Formisano, P.-A. Lindqvist, C. C. Cattell, F. Mozer, and R. Torbert, Quasistatic electric field measurements with spherical double probes on GEOS and ISEE satellites, *Space Sci. Rev., 37*, 269, 1984.

Reiff, P. H., H. L. Collin, E. G. Shelley, J. L. Burch, and J. D. Winningham, Heating of upflowing ionospheric ions on auroral field lines, in *Ion Acceleration in the Magnetosphere and Ionosphere, Geophys. Monogr. Ser.*, vol. 38, edited by T. Chang, p. 83, AGU, Washington, D. C., 1986.

Reiff, P. H., H. L. Collin, J. D. Craven, J. L. Burch, J. D. Winningham, E. G. Shelley, L. A. Frank, and M. A. Friedman, Determination of auroral electrostatic potentials using high- and low-altitude particle distributions, *J. Geophys. Res., 93*, 7441, 1988.

Roth, I., M. K. Hudson, and R. Bergmann, Effects of ion two-stream instability on auroral ion heating, *J. Geophys. Res., 94*, 348, 1989.

Russell, C. T., The ISEE 1 and 2 fluxgate magnetometers, *IEEE Trans. Geosci. Electron., GE-16*, 239, 1978.

Sharp, R. D., W. Lennartsson, W. K. Peterson, and E. Ungstrup, The mass dependence of wave particle interactions as observed with the ISEE-1 ion mass spectrometer, *Geophys. Res. Lett., 10*, 651, 1983.

Shelley, E. G., R. D. Sharp, R. G. Johnson, J. Geiss, P. Eberhardt, H. Balsiger, G. Haerendel, and H. Rosenbauer, Plasma composition experimentation on ISEE-A, *IEEE Trans. Geosci. Electron., GE-16*, 266, 1978.

Temerin, M. A., and R. L. Lysak, Electromagnetic ion cyclotron mode (ELF) waves generated by auroral electron precipitation, *J. Geophys. Res., 89*, 2849, 1984.

Temerin, M. A., and F. S. Mozer, Observations of the electric fields that accelerate auroral particles, *Proc. Indian Acad. Sci., 93*, 227, 1984.

Temerin, M. A., M. Woldorff, and F. S. Mozer, Nonlinear steepening of the electrostatic ion cyclotron wave, *Phys. Rev. Lett., 43*, 1941, 1979.

Temerin, M. A., C. A. Cattell, R. L. Lysak, M. K. Hudson, R. B. Torbert, F. S. Mozer, R. D. Sharp, and P. M. Kintner, The small-scale structure of electrostatic shocks, *J. Geophys. Res., 86*, 11,278, 1981.

Tetreault, D., Theory of electric fields in the auroral acceleration region, *J. Geophys. Res., 96*, 3549, 1991.

Ungstrup, E., D. M. Klumpar, and W. J. Heikkila, Heating of ions to superthermal energies in the topside ionosphere with electrostatic ion cyclotron waves, *J. Geophys. Res., 84*, 4289, 1979.

Winglee, R. M., P. B. Dusenbery, H. L. Collin, C. S. Lin, and A. M. Persoon, Simulations and observations of heating of auroral ion beams, *J. Geophys. Res., 94*, 8943, 1989.

R. R. Anderson, Department of Physics and Astronomy, University of Iowa, Iowa City, IA 52242.

C. A. Cattell, F. S. Mozer, and I. Roth, Space Sciences Laboratory, University of California, Berkeley, CA 94720.

R. C. Elphic, Los Alamos National Laboratory, Los Alamos, NM 87545.

W. Lennartsson, Lockheed Palo Alto Research Laboratory, Palo Alto, CA 94304.

E. Ungstrup, Danish Space Research Institute, Lundtoft Vej 7 DK-2800, Lyngby, Denmark.

(Received July 16, 1990;
revised January 29, 1991;
accepted January 30, 1991.)